X-ray diffraction study on the effects of hydrogen on Pd60Cu40 wt% foil membranes

Al-Mufachi, Naser; Steinberger-Wilckens, Robert

DOI:
10.1016/j.memsci.2017.09.084

Document Version
Peer reviewed version

Citation for published version (Harvard):
Al-Mufachi, N & Steinberger-Wilckens, R 2018, 'X-ray diffraction study on the effects of hydrogen on $Pd_{60}Cu_{40}$ wt% foil membranes', *Journal of Membrane Science*, vol. 545, pp. 266-274.
https://doi.org/10.1016/j.memsci.2017.09.084

X-ray diffraction study on the effects of hydrogen on $Pd_{60}Cu_{40}$ wt% foil membranes

N.A. Al-Mufachi*, R. Steinberger-Wilckens

Centre for Hydrogen and Fuel Cell Research, School of Chemical Engineering, University of Birmingham, Edgbaston B15 2TT, UK

*Corresponding author:
E-mail address: n.a.al-mufachi@bham.ac.uk
Tel: + 44 121 414 5081

Abstract

In-situ variable temperature X-ray diffraction analysis was performed on two as-received $Pd_{60}Cu_{40}$ wt% foil samples containing the disordered face centred cubic (FCC) phase between 30 and 700 °C. One foil sample was exposed to 445 kPa of flowing helium and the other foil sample was exposed to 445 kPa of flowing hydrogen. Generally, it was found that 445 kPa of flowing hydrogen had the effect of expanding the temperature range over which the body centred cubic (BCC) phase in the foil sample was stable when compared to testing under 445 kPa of flowing helium. This is likely due to dissolved hydrogen shifting the BCC | FCC + BCC and FCC + BCC | FCC phase boundaries to relatively higher temperatures and Pd contents.

An as-received $Pd_{60}Cu_{40}$ wt% foil membrane had been cycled from 50 to 450 °C under a 445 kPa feed pressure and 100 kPa permeate pressure of hydrogen. In the third cycle, this membrane achieved a noticeably low hydrogen permeability of 5.59×10^{-9} mol m^{-1} s^{-1} $Pa^{-0.5}$ at 450 °C. Moreover, the partial pressure exponent was found to deviate significantly from Sieverts' law between 400 and 450 °C. Subsequently, this membrane was cycled twice between 250 and 700 °C achieving a much higher hydrogen permeability of 1.19×10^{-8} mol m^{-1} s^{-1} $Pa^{-0.5}$ which was measured at 450 °C. The activation energy for permeation reduced by more than 60% and the partial pressure exponent decreased to 0.52. The initial poor hydrogen permeability of the membrane was attributed to coring as evidenced by the presence of the disordered FCC phase in the as-received foil. The improvement in hydrogen permeability was linked to the homogenisation effect of hydrogen under the conditions used in this study.

Keywords

Pd-Cu foil membrane
Dense metal membrane

Hydrogen separation
X-ray diffraction
Hydrogen permeability

1 Introduction

The large majority of commercial hydrogen gas is produced using the steam methane reforming process [1]. With the expected expansion in the polymer electrolyte fuel cell industry, it is anticipated that there will be an associated growth in demand for high-purity hydrogen (99.999%) [2, 3]. Pd-based dense alloy foil membranes, such as Pd-Cu and Pd-Ag, are used for hydrogen separation applications as a result of their high catalytic activity for the dissociation of hydrogen molecules, excellent hydrogen permeation, mechanical strength and durability [4-6]. The Pd-Cu alloy system has garnered much attention over the years since Cu additions greatly lower cost and the presence of the Pd-rich Pd-Cu FCC phase provides improved tolerance to hydrogen sulphide contamination when compared to other dense metallic membranes available on the market [7-12].

The Pd-Cu phase diagram shown in Fig. 1 reveals that below a temperature of 450 °C the $Pd_{60}Cu_{40}$ wt% composition has a purely ordered CsCl-type BCC crystal structure [13]; and this composition has been shown [4, 7, 8, 12, 14, 15] to have the maximum hydrogen permeability within the entire alloy system. A 3 wt% deviation from this optimal composition can substantially decrease hydrogen permeability by a minimum of 50% [16]. Therefore, $Pd_{60}Cu_{40}$ wt% foil membranes were chosen for this study and any further mention of Pd-Cu foil membranes within this article shall be of this composition unless stated otherwise.

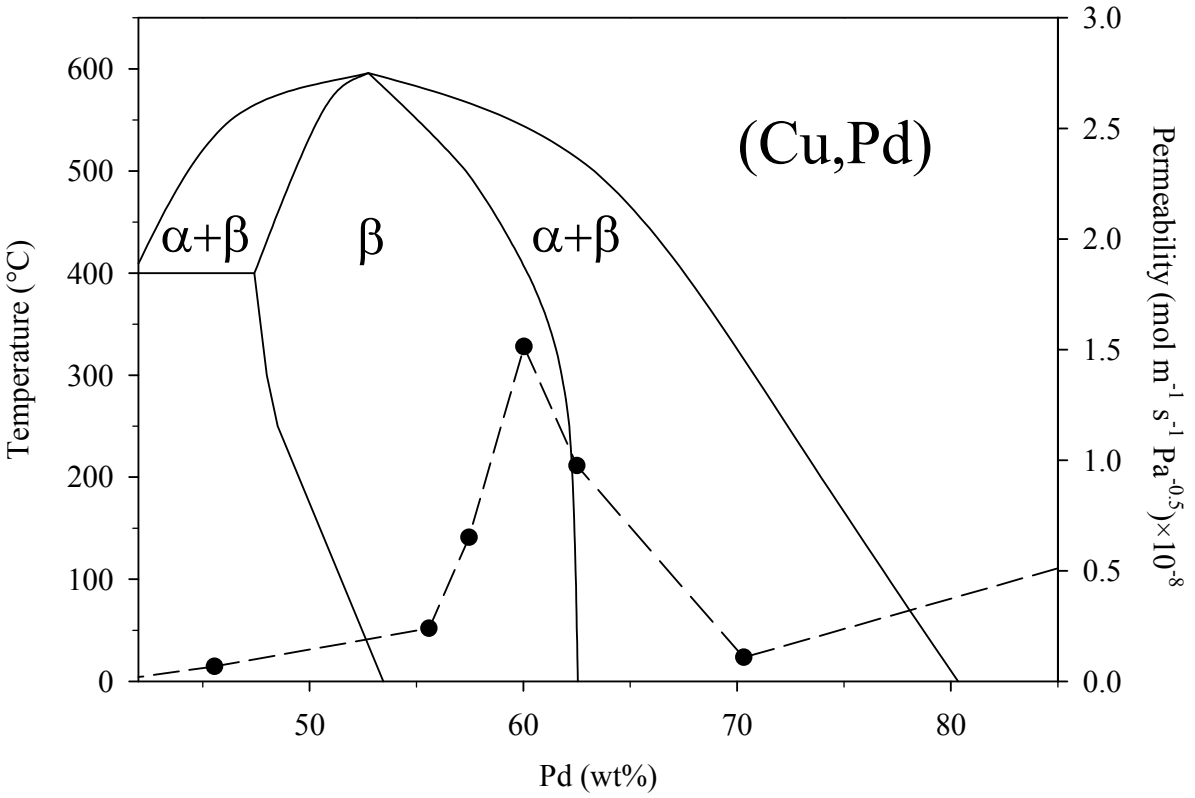

Fig. 1 The Pd-Cu phase diagram where 'α' indicates the disordered FCC phase and 'β' indicates the ordered BCC phase. This phase diagram was produced using literature data [13, 17] and includes a curve of hydrogen permeability as a function of Pd concentration at 350 °C plotted using data from Howard et al [15].

Hydrogen diffusivity in the Pd-Cu system is two orders of magnitude higher in the BCC phase in comparison to the FCC phase [14, 15, 18, 19]. For a composition of $Pd_{60}Cu_{40}$ wt% and at temperatures greater than 450 °C, the FCC phase starts to form and is the only equilibrium phase present above 600 °C. It has been reported by Piper [14] that dissolved hydrogen has the ability to move the BCC | FCC + BCC phase boundary to relatively higher Pd concentrations. Hydrogen pressures between 0 and 0.51 MPa seem to move this phase boundary much more relative to pressures ranging from 0.51 to 12.16 MPa. A similar phenomenon has been reported by Huang et al [20] whereby dissolved hydrogen was treated as an additional alloying element.

Other work has presented evidence to suggest that atomic diffusion and rearrangement is accelerated in the presence of hydrogen [21, 22]. It was noted by Decaux [23], that a ~$Pd_{60}Cu_{40}$ wt% foil annealed at 200 °C under vacuum revealed no indication of the equilibrium BCC phase, although, a mixed FCC and BCC phase formed upon annealing for 26 hours at 250 °C under a hydrogen pressure of 100 kPa. Hydrogen has been shown to have other notable effects on the Pd-Cu alloy system, for example temperature cycling of ~$Pd_{60}Cu_{40}$ wt% membranes through the miscibility gap can result in permeation hysteresis [16, 24]. It has been observed that transition of a Pd-Cu FCC alloy membrane into the mixed FCC + BCC phase was retarded throughout the cooling stage which was in contrast to the heating stage of the cycle [16].

The aim of this work is to examine the effects of hydrogen and elevated temperatures on a $Pd_{60}Cu_{40}$ wt% foil membrane using ex-situ and in-situ X-ray diffraction techniques. This will yield a better understanding of the hydrogen permeability test conditions used in this work on phase formation and stability as well as effects on the kinetics of the separation process.

2 Experimental

2.1 Sample preparation

Johnson Matthey Noble Metals (Royston, UK) supplied the 31.0 ± 0.8 µm thick cold rolled Pd-Cu foil used in this work. A circular membrane disc with a 21 mm diameter and two square samples with an approximate area of 25 mm^2 (Foils 1 and 2) were cut from the same as-received Pd-Cu foil and subsequently degreased in acetone using an ultrasonic bath for 5 minutes.

2.2 Hydrogen permeability measurement

An inhouse built membrane permeability rig (MPR) was used for conducting hydrogen permeability measurements of the Pd-Cu foil membrane. The membrane was mounted inside an Inconel reactor which maintained a hermetic seal throughout the entire experiment. The reactor was evacuated down to ~10^{-6} kPa using a Pfeiffer TSU-071E turbomolecular drag high vacuum pumping system with a membrane backing pump. The gas inlet to the hermetically sealed membrane feed side was regulated using a Brookes 5850S Mass Flow Controller (MFC). A continuous flow of hydrogen gas was used and released through an additional MFC in order to maintain a constant hydrogen feed pressure and prevent accumulation of impurities. A third MFC had the task of measuring the flow of hydrogen on the permeate side of the membrane. Hydrogen permeability in the FCC phase was significantly low so that the downstream MFC had difficulty detecting any hydrogen permeation at times since the device was calibrated to measure only as low as 6 ± 6 ml min^{-1} of hydrogen gas flow. With such large error for small gas flows, the activation energy could not be accurately determined.

An Elite Thermal Systems Ltd split furnace was used to heat the reactor and membrane to the desired temperatures which was monitored using Inconel K-type thermocouples. A PC and SpecView software was responsible for controlling the MFCs, split furnace and logging of data. During MPR testing of the Pd-Cu foil membrane, the heating and cooling rate was 2 °C min^{-1} and approximately 0.5 °C min^{-1}, respectively. This cooling rate was achieved by allowing the MPR to naturally furnace cool.

The Pd-Cu foil membrane was supported atop of a porous stainless steel disc inside the reactor to help avoid any mechanical deformation caused as a result of the applied pressure differential used during MPR testing. The pore size of the porous stainless steel support ranged between 10 and 20 µm. Additionally, 1 mm diameter holes were drilled into the support to help reduce flow resistance on the downstream end. During MPR testing, a

hydrogen feed and permeate pressure of 445 and 100 kPa, respectively, were applied. The hydrogen gas used in this work was supplied by Air Products with a purity of 99.99996%. Initially, the Pd-Cu foil membrane was cycled thrice from 50 to 450 °C. Subsequently, the Pd-Cu foil membrane performed two cycles between 250 and 700 °C in order to record the hydrogen permeability of the disordered FCC phase and to homogenise the membrane.

The partial pressure exponent (*n*-value) was determined by measuring the hydrogen flux through the Pd-Cu foil membrane isothermally under various feed pressures. This experiment was performed after the Pd-Cu foil membrane had undergone the initial three cycles from 50 to 450 °C and again following the completion of two cycles from 250 to 700 °C. These experiments were conducted at 350, 375, 400, 425 and 450 °C whilst hydrogen flux measurements were taken at feed pressures of 300, 400, 500, 600 and 700 kPa at each temperature. A constant hydrogen pressure of 100 kPa was maintained on the permeate side of the membrane during each experiment. The coefficient of determination (R^2) for the fitted regression line of the data was used to determine the *n*-value.

2.3 X-ray diffraction analysis

Ex-situ X-ray diffraction (XRD) analysis of either sides of the Pd-Cu foil membrane was carried out under ambient conditions both before and after MPR testing in order to examine any phase or compositional changes resulting from the experimental conditions. The XRD machine used in this work was a Bruker D8-Advance diffractometer which used a monochromatic $CuK_{\alpha 1}$ radiation with a wavelength of 1.54056 Å.

The Pd-Cu FCC lattice parameter was determined from the ex-situ XRD patterns acquired for the as-received foil. To do this, the lattice parameter is computed for each diffraction peak using Bragg's law. Then, these lattice parameter values are plotted as a function of $\cos^2\theta$ (θ is the Bragg angle) whereby the *y*-intercept of this straight-line plot gives the absolute lattice parameter. This method has been described in detail by Cullity [25].

In-situ variable temperature XRD (VTXRD) analyses was conducted on Foils 1 and 2 with an Anton Paar XRK 900 pressure cell to detect any phase transformations that may occur under conditions similar to those used during MPR testing. 445 kPa of flowing helium was used during the analysis of Foil 1 in order to identify the phase transition temperatures in an inert environment and for comparison Foil 2 was exposed to 445 kPa of flowing hydrogen. Air Products also supplied the helium gas used in this experiment which had a purity of 99.9999%. The goal was to study the influence of hydrogen on phase transformation in the Pd-Cu alloy system under similar conditions to those used during MPR testing. VTXRD scans were captured at fixed temperatures prior to heating to the subsequent temperature set point. The VTXRD experiments were performed between 25 and 700 °C using a heating and cooling rate of 2.4 °C min^{-1} and 5 °C min^{-1}, respectively.

2.4 Scanning electron microscopy/Energy dispersive spectroscopy analysis

A Joel 6060 microscope equipped with INCA EDAX software was used to perform scanning electron microscopy (SEM) and energy dispersive spectroscopy (EDS) on the as-received Pd-Cu foil in secondary electron imaging mode for determining chemical composition.

3 Results and discussion

3.1 Initial ex-situ XRD and in-situ VTXRD analyses

The composition of the as-received Pd-Cu foil was nominally $Pd_{60}Cu_{40}$ wt%. The Pd-Cu phase diagram shown in Fig. 1 indicates that a purely ordered BCC equilibrium phase is stable below 450 °C for a composition of $Pd_{60}Cu_{40}$ wt%. Representative ex-situ XRD patterns of the as-received Pd-Cu foil are shown in Fig. 2 confirming the presence of the disordered FCC phase that maybe the result of quenching of the alloy melt from the molten state thus trapping this high temperature phase. Additionally, Fig. 2(a) displays a diffraction peak at a 2θ value of 29.4° which matches with the $Cu_2O(110)$ diffraction peak. It seems likely that the Cu used to produce this foil would have formed a passive oxide film before melting which could be responsible for the appearance of this oxide peak.

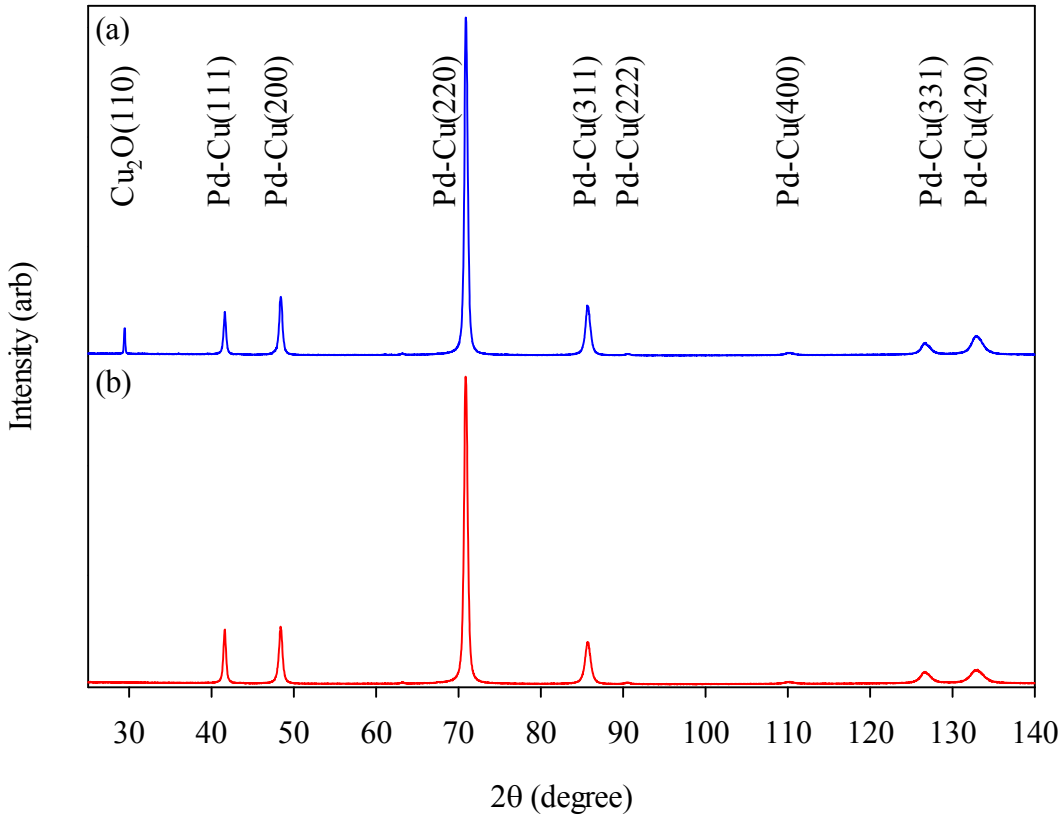

Fig. 2 Representative ex-situ XRD patterns of the Pd-Cu foil membrane in the as-received state acquired for the (a) feed side and (b) permeate side prior to MPR testing.

From the XRD data shown in Fig. 2, an average lattice parameter of 3.7565 Å was determined for the FCC phase which corresponds to a composition of $Pd_{61.3}Cu_{38.7}$ wt%. Phase composition was calculated based on Vegard's law [26] using Eq. 1 where a is crystal lattice parameter in Å and x_{Pd} is the Pd concentration in at%. Eq. 1 has been derived from data presented in an earlier article with a greater degree of accuracy than previously reported [27]. EDS chemical analysis revealed an average foil composition of $Pd_{60.3}Cu_{39.7}$ wt%.

$$a = (2.7522 \times 10^{-3})x_{Pd} + 3.6226 \quad \text{Eq. 1}$$

VTXRD experiments were performed on Foils 1 and 2 in the as-received state. Initially, Foil 1 was cycled under flowing helium at a pressure of 445 kPa throughout the VTXRD experiment for the purpose of determining the phase transition temperature in a hydrogen-free inert atmosphere. Fig. 3 reveals the heating stage of the cycle from 250 to 700 °C. From 250 to 500 °C, XRD scans were acquired at 25 °C increments for the purpose of capturing sudden phase transitions. XRD scans were recorded at 50 °C increments above 500 °C all the way to the maximum temperature of 700 °C. Foil 1 is shown to contain a purely disordered FCC phase at room temperature as indicated by 'α'. 'β' indicates the BCC phase which begins formation at 300 °C and shows signs of being fully ordered by 475 °C as demonstrated at 2θ = 30° by the BCC Pd-Cu(100) diffraction peak. The corundum sample holder is denoted by 'c'. The FCC phase no longer appears at 325 °C showing only signs of the BCC phase, however the FCC phase forms again at 475 °C. Above 600 °C, the BCC phase no longer appears indicating only the presence of the FCC phase up until the end of the cycle at 700 °C.

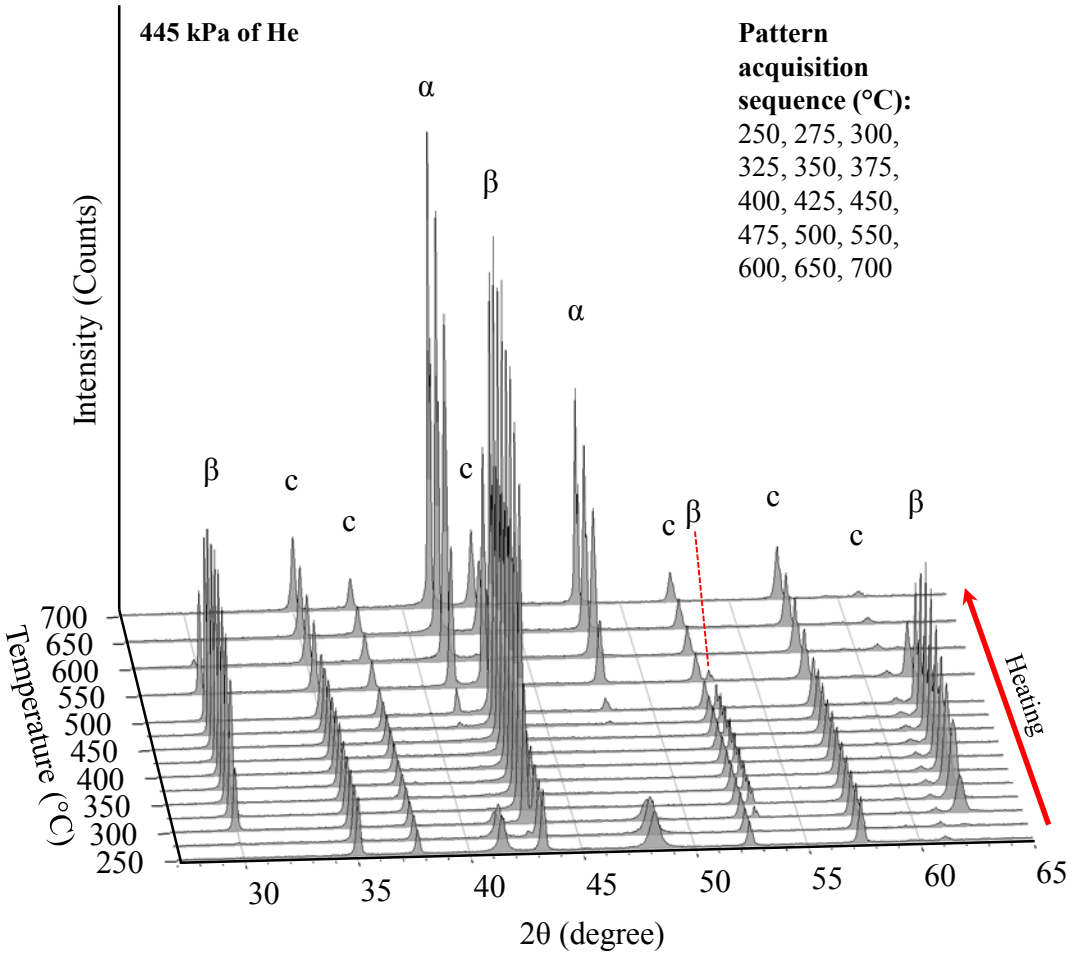

Fig. 3 VTXRD patterns of Foil 1 displaying the heating stage of the cycle exposed to flowing helium at a pressure of 445 kPa, whereby 'α', 'β' and 'c' represent the diffraction peaks associated with the FCC phase, BCC phase and corundum sample holder, respectively.

Fig. 4 shows the VTXRD results throughout the cooling stage which proceeded the heating stage of the cycle shown in Fig. 3, whereby scans were acquired at 50 °C increments.

As shown in Fig. 4, Foil 1 contains mainly the FCC phase between 700 and 450 °C. Then the BCC phase emerges in Foil 1 at 450 °C to give rise to a mixed phase. Subsequently at 300 °C, the BCC phase shows signs of being completely ordered and the presence of the FCC phase significantly diminishes, although small traces are still evident.

Upon reaching room temperature, minute quantities of the FCC phase remain stable in Foil 1 which could be the result of the relatively quick cooling rate of 5 °C min^{-1} experienced by the VTXRD pressure cell. In contrast, the MPR is able to achieve relatively slower cooling rates of approximately 0.5 °C min^{-1}. In order to promote the complete phase transformation of the FCC phase to the BCC phase, a slow cooling rate is necessary. However, this proved challenging to accomplish with a water-cooled pressure cell hence creating unsuitable conditions for the formation of a pure BCC equilibrium phase in Foil 1 at room temperature.

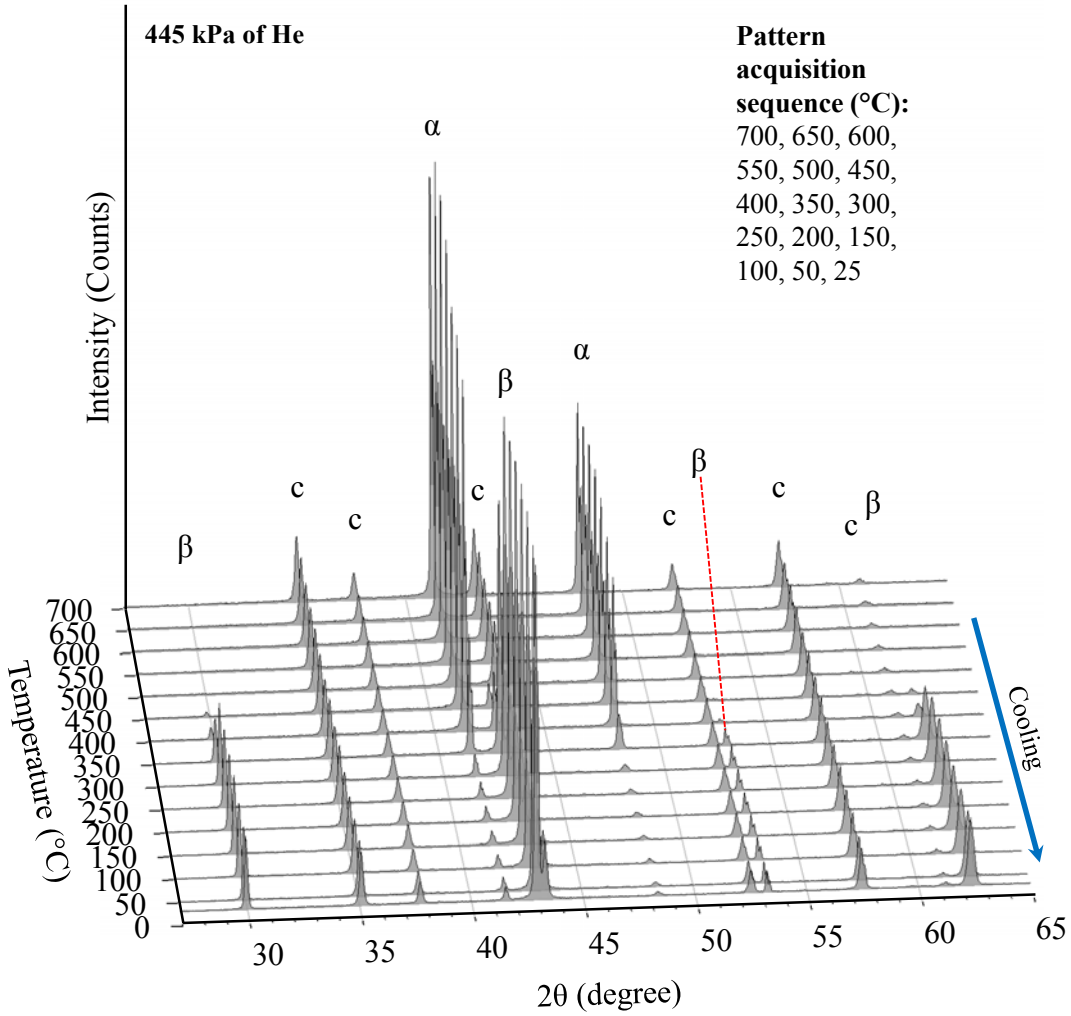

Fig. 4 VTXRD patterns of Foil 1 displaying the cooling stage of the cycle exposed to flowing helium at a pressure of 445 kPa. Note that the final pattern is acquired at 25 °C.

The VTXRD data shown in Fig. 3 and Fig. 4 are compiled in Table 1. Clear evidence is shown that the BCC phase is stable from 300 to 600 °C during heating of Foil 1 under 445 kPa of flowing helium. The Pd-Cu phase diagram displayed in Fig. 1 demonstrates that for the $Pd_{60}Cu_{40}$ wt% composition, the FCC + BCC | FCC phase boundary resides at 550 °C. Subramanian [13], Huang [20] and Li [17] have each constructed the Pd-Cu phase diagram

based on data from Jones [28] showing that for the $Pd_{60}Cu_{40}$ wt% composition, the FCC + BCC | FCC phase boundary occurs at 550 °C. These authors indicate that the BCC phase is not stable above temperatures of 550 °C; yet, Fig. 3 shows evidence that under the VTXRD experimental conditions used the BCC phase is present up to 600 °C.

At 450 °C, the BCC phase appears in Foil 1 in the cooling stage signifying that the FCC + BCC | FCC phase boundary has relocated to a relatively lower temperature. This finding could be associated with the relatively fast cooling rate experienced by Foil 1 which would likely not enable the BCC phase to form at a comparable temperature observed in the heating stage. A relatively slower cooling rate would be expected to increase the temperature at which the BCC phase forms in the cooling stage.

VTXRD analysis was performed on the as-received Foil 2 under flowing hydrogen at a pressure of 445 kPa using the identical cycle programme used for Foil 1. The VTXRD analysis results for Foil 2 are displayed in Table 1. Fig. 5 reveals that the BCC phase appears at 275 °C and achieves complete ordering by 400 °C as indicated by the BCC Pd-Cu(100) diffraction peak. The VTXRD experiment aims to emulate MPR testing conditions, although it must be noted that a hydrogen pressure gradient is not applied across Foil 2 in the experiment. It should be pointed out that the VTXRD and MPR experiments have been performed under non-equilibrium conditions. Therefore, measurements and observations from these experiments could change under equilibrium conditions.

Hydrogen seems to have a noticeable influence on the Pd-Cu phase diagram. Fig. 5 demonstrates that in Foil 2, which has a composition of $Pd_{61.3}Cu_{38.7}$ wt%, the FCC phase starts appearing at 500 °C to produce the mixed FCC + BCC phase. At 650 °C, the BCC phase no longer appears. Fig. 1 shows that at a composition of $Pd_{61.3}Cu_{38.7}$ wt% and at 450 °C, Foil 2 is expected to reside in the mixed FCC + BCC phase region near to the BCC | FCC + BCC phase boundary. Moreover, Fig. 5 demonstrates that 445 kPa of flowing hydrogen repositions the BCC | FCC + BCC and FCC + BCC | FCC phase boundaries to greater temperatures. Piper [14] reports a similar observation suggesting that greater shifts in the phase boundaries to the Pd-rich end of the Pd-Cu phase diagram are seen at elevated hydrogen pressures. Furthermore, higher hydrogen pressures are capable of stabilising the BCC phase to higher than expected Pd concentrations. Matsumura [29] also reports findings on $Pd_{54}Cu_{46}$, $Pd_{56}Cu_{44}$, and $Pd_{60}Cu_{40}$ wt% foil membranes demonstrating that the presence of hydrogen can expand the BCC phase boundary to higher Pd concentrations and higher than normal temperatures. It is evident that the BCC phase is stabilised over a greater temperature range (275 – 650 °C) in Foil 2 when compared to Foil 1 (300 – 600 °C). During heating, the FCC phase does not form at the same temperature (325 °C) and also reappears at a higher temperature (500 °C) in Foil 2 when compared to Foil 1.

In general, it has been observed that for a composition of $Pd_{61.3}Cu_{38.7}$ wt% exposed to 445 kPa of hydrogen pressure and a heating rate of 2.4 °C min^{-1}, the BCC | FCC + BCC phase boundary shifts from 340 to 500 °C and the FCC + BCC | FCC phase boundary shifts from 530 to 650 °C. This is evidence that 445 kPa of hydrogen pressure is able to accelerate the FCC to BCC phase transformation and stabilise the BCC phase to higher temperatures as well as reduce the temperature range over which the mixed FCC + BCC phase exists from 190 °C to 150 °C.

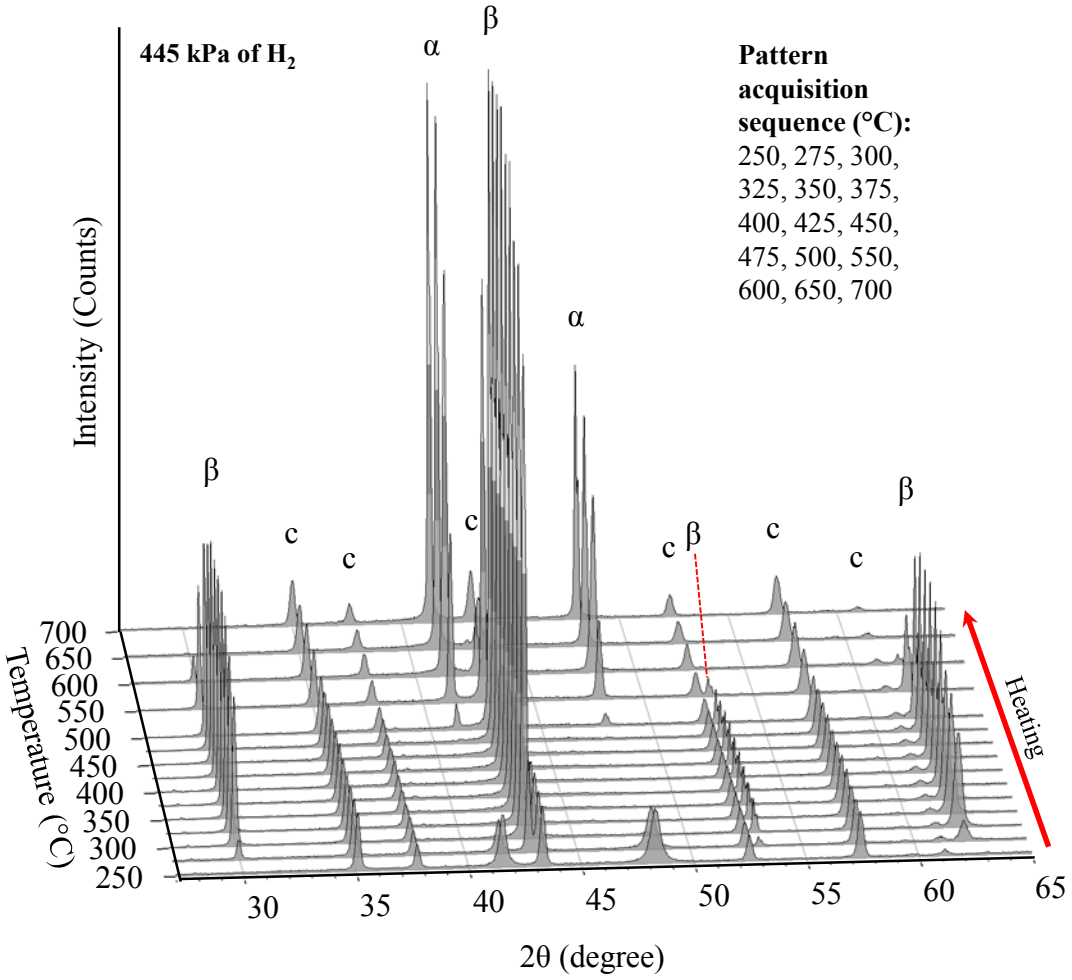

Fig. 5 VTXRD patterns of Foil 2 displaying the heating stage of the cycle exposed to flowing hydrogen at a pressure of 445 kPa.

Fig. 6 shows the cooling stage of the cycle for Foil 2. In Foil 2, the FCC phase forms between 700 and 30 °C, however similar to Foil 1, there is a substantial reduction at 300 °C in the presence of the FCC phase. At 500 °C, the BCC phase forms in Foil 2 during the cooling stage while the same phase forms in Foil 1 at 450 °C providing further evidence that 445 kPa of flowing hydrogen pressure accelerates the FCC to BCC phase transitions. Additionally, Foil 2 seems to achieve a completely ordered BCC phase by 275 °C which is comparatively lower than the Foil 1 ordering temperature (300 °C) in the heating stage implying that hydrogen can accelerate the rate of ordering in Pd-Cu BCC phase.

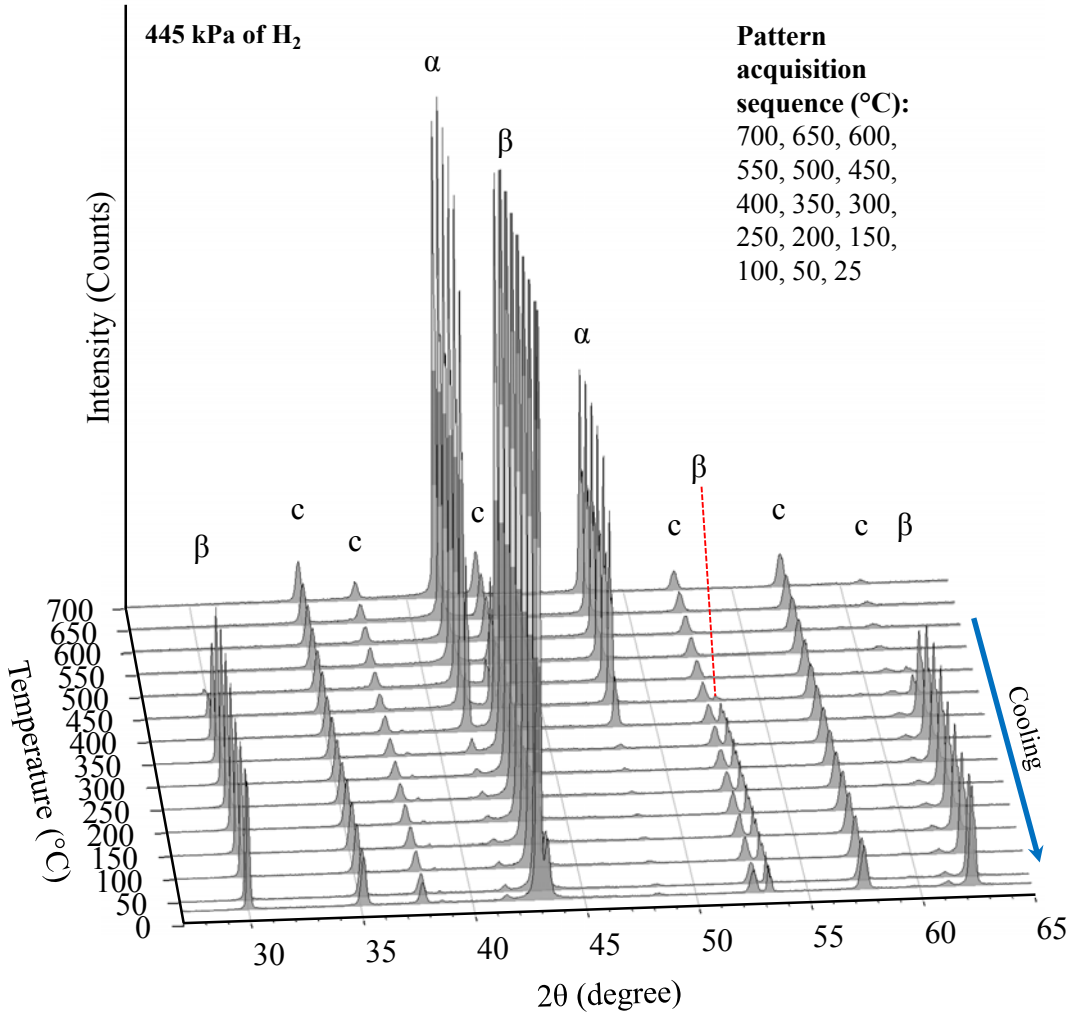

Fig. 6 VTXRD patterns of Foil 2 displaying the cooling stage of the cycle exposed to flowing hydrogen at a pressure of 445 kPa. Note that the final pattern is acquired at 25 °C.

Table 1 Summary of VTXRD experimental results for Foils 1 and 2 which were cycled from 30 – 700 – 30 °C. Foil 1 was exposed to flowing helium at a pressure of 445 kPa and Foil 2 was exposed to flowing hydrogen at a pressure of 445 kPa. Temperatures are listed at which the FCC and BCC phase appear in the heating and cooling stage of the cycle.

		Heating stage (2.4 °C min^{-1} heating rate)	Cooling stage (5 °C min^{-1} cooling rate)
Foil 1	FCC	30 – 325 °C, 475 – 700 °C	700 – 30 °C
	BCC	300 – 600 °C	450 – 30 °C
Foil 2	FCC	30 – 325 °C, 500 – 700 °C	700 – 30 °C
	BCC	275 – 650 °C	500 – 30 °C

3.2 MPR results

At first, the MPR was used to measure the hydrogen permeability of the Pd-Cu foil membrane from 50 to 450 °C. Fig. 7 shows that hydrogen permeation was initially detected at 410 °C during the first cycle. It is acknowledged that hydrogen permeation could be taking place at lower temperatures than observed especially if the gas flow rate is below the detection limit of the downstream MFC. The initial cycle anneals the Pd-Cu foil

membrane and promotes the phase transition from the FCC phase BCC phase. For the MPR test conditions used during this study, only the ordered BCC phase is present at 410 °C which is corroborated well by the VTXRD data displayed in Fig. 5. The presence of hydrogen would facilitate rapid ordering of the BCC phase [21, 22, 30, 31] since local rearrangement of the Pd and Cu atoms is only necessary. Additionally, it can be seen that hydrogen permeation was first detected at 370 °C for the second cycle and 350 °C for the third cycle.

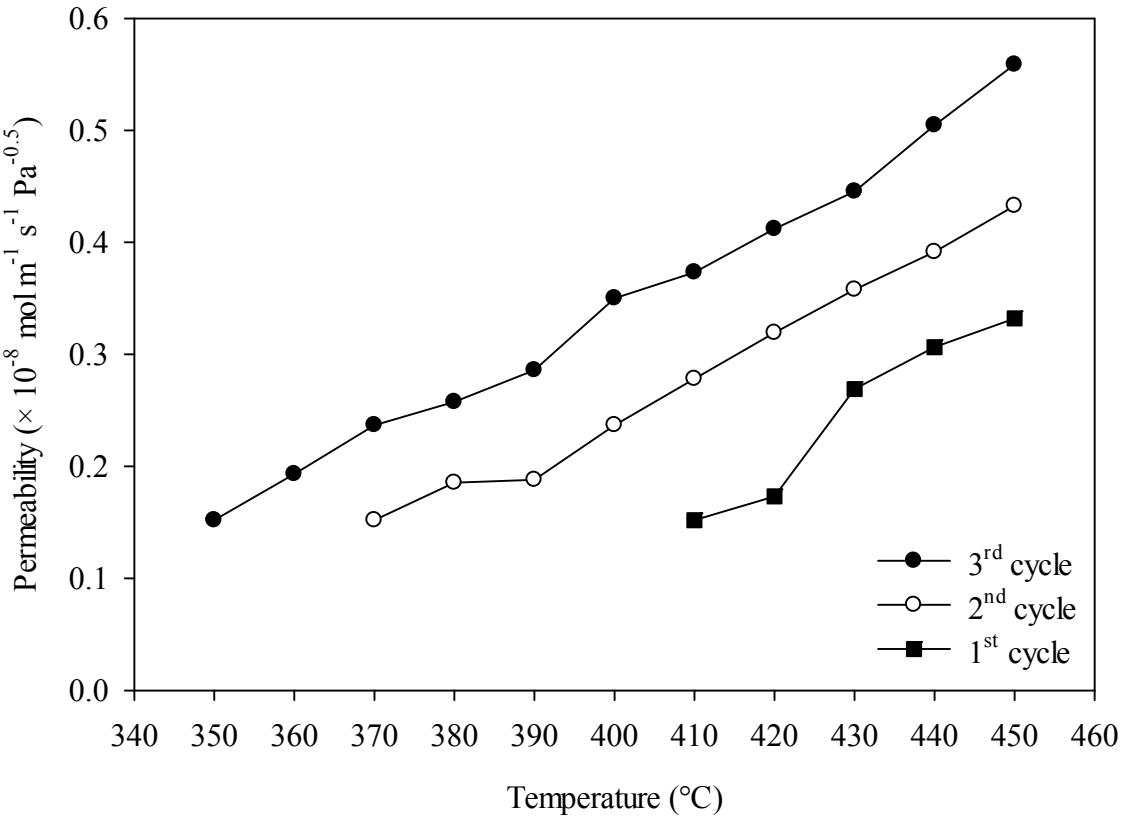

Fig. 7 Hydrogen permeability results for the as-received Pd-Cu foil membrane with a thickness of 31.0 µm displaying the initial three cycles heated from 50 to 450 °C. A hydrogen feed pressure of 445 kPa and permeate pressure of 100 kPa was used throughout the MPR test.

Hydrogen diffusion in the Pd-Cu BCC phase is comparatively faster than in the Pd-Cu FCC phase [13, 32, 33] and thus has a relatively higher hydrogen permeability. Piper [14] and Huang [20] have demonstrated that the BCC | FCC + BCC phase boundary can move to higher Pd concentrations with increasing hydrogen pressure. Note that the membrane feed side is subjected to a hydrogen pressure of 445 kPa while the permeate side is exposed 100 kPa of hydrogen pressure. Therefore, it is anticipated for the composition of the Pd-Cu foil membrane that more of the FCC phase is transformed to the BCC phase on the feed side when compared to the permeate side during MPR testing. Fig. 13(b) presents evidence for this whereby minute traces of the FCC phase are detected on the membrane permeate side as indicated by the Pd-Cu(111) diffraction peak for the Pd-Cu foil membrane which was cycled thrice from 50 to 450 °C in the MPR subsequent to removal.

Transformation from the less permeable FCC phase to the more permeable BCC phase continues on the membrane permeate side with each successive cycle until the FCC

phase no longer remains. This would help to explain the detection of hydrogen permeation at lower temperatures with each consecutive cycle.

It has previously been proposed that fast phase transformation is the consequence of rapid atomic diffusion resulting from the development of vacancy-hydrogen clusters [21, 22, 34, 35] which essentially occurs when metal vacancies trap hydrogen atoms. Since the membrane feed side is exposed to relatively higher hydrogen pressures, it will undergo a much faster phase transformation from the disordered FCC phase to the ordered BCC phase.

The *n*-value of a dense metal membrane is a significant parameter as it can give information on the kinetics of the separation process. According to Sieverts' law (Eq. 2), the concentration of a dissolved gas in a metal (C) is proportional to the square root of the partial pressure of the gas (P) in thermodynamic equilibrium (S denotes the solubility constant). Therefore, Sieverts' law assumes that the *n*-value is 0.5. An *n*-value of approximately 0.5 indicates hydrogen dissociation occurs relatively fast and hydrogen diffusion is relatively slow. Conversely, if the *n*-value tends to unity then hydrogen dissociation becomes the rate limiting step. However, other aspects could be the cause of the *n*-value deviating from Sieverts' law such as recombinative hydrogen desorption, non-ideal hydrogen diffusion, surface contamination and the influence of support materials [36].

$$C = SP^{1/2} \qquad \textbf{Eq. 2}$$

Fig. 8 shows *n*-value measurements conducted on the Pd-Cu foil membrane subsequent to MPR testing. A best fit *n*-value of 0.58 is obtained for the data displayed in Fig. 8, demonstrating that hydrogen permeation in the Pd-Cu foil membrane is limited by the diffusion process for the test conditions used.

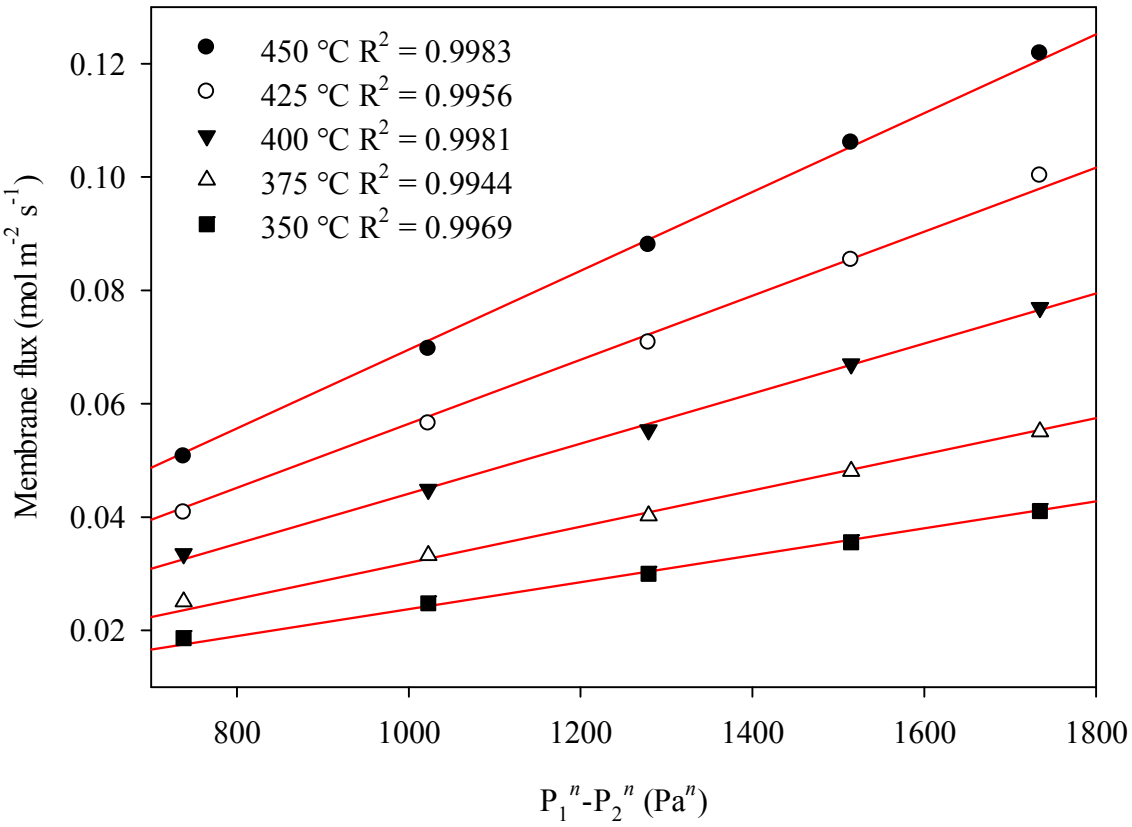

Fig. 8 Membrane flux against hydrogen differential pressure constrained to the best fit *n*-value of 0.58.

Hydrogen permeability is a temperature dependent parameter, denoted as Φ, which is represented in the following Arrhenius-type Eq. 3:

$$\Phi = \Phi_0 exp\left(\frac{-E_\Phi}{RT}\right) \quad \textbf{Eq. 3}$$

where Φ_0 is the maximum permeability at infinitely high temperatures, E_Φ is the activation energy for hydrogen permeation, R is the universal gas constant and T is temperature. The general permeability formulae (350 – 450 °C) for the Pd-Cu foil membrane for an *n*-value of 0.5 and best fit *n*-value of 0.58 are given in Eq. 4 and Eq. 5, respectively.

$$\Phi_{n=0.5} = (2.88 \times 10^{-5})\ mol\ m^{-1}\ s^{-1}\ Pa^{-0.5} \times exp\left(\frac{-51.09\ kJ\ mol^{-1}}{RT}\right) \quad \textbf{Eq. 4}$$

$$\Phi_{n=0.58} = (8.87 \times 10^{-6})\ mol\ m^{-1}\ s^{-1}\ Pa^{-0.58} \times exp\left(\frac{-51.09\ kJ\ mol^{-1}}{RT}\right) \quad \textbf{Eq. 5}$$

At 350 °C during the third cycle, the hydrogen permeability of the Pd-Cu foil membrane was found to be 1.52×10^{-9} mol m^{-1} s^{-1} $Pa^{-0.5}$. This hydrogen permeability value is comparatively low upon comparison with literature data displayed in Table 2. Although, it is

important to consider that these hydrogen permeability values shown in Table 2 do not agree well with each other as they widely vary between 0.50 and 1.76×10^{-8} mol m^{-1} s^{-1} $Pa^{-0.5}$.

Table 2 Hydrogen permeability of free-standing $Pd_{60}Cu_{40}$ wt% foil membranes at 350 °C.

Hydrogen permeability ($\times 10^{-8}$ mol m^{-1} s^{-1} $Pa^{-0.5}$)	Reference
1.42	Decaux [23]
0.50	Howard [15]
0.60	Kamakoti [37]
1.07 1.76[a]	Krueger [38]
1.49	McKinley [8]

[a] denotes measurement recorded following heat treatment of the alloy membrane.

A possible cause for the low hydrogen permeability displayed by the as-received Pd-Cu foil membrane is elucidated by Krueger [38] who mentions that homogenisation of an as-received $Pd_{60}Cu_{40}$ wt% foil membrane for 40 minutes at 1,100 °C in a mildly reducing atmosphere can yield up to a 65% improvement in hydrogen permeability. This improvement has been attributed to a coring process. Quenching an alloy melt from the molten phase can result in the external region solidifying at a much higher rate than the internal region. Grains formed in the internal region have a larger concentration of the constituent with the highest melting point; in this instance Pd, whilst the external region contain grains which are depleted with Pd thus creating compositional inhomogeneity in the alloy [38]. The inhomogeneity in the Pd-Cu foil membrane can be detrimental to its performance because hydrogen permeability is affected by phase composition as demonstrated in Fig. 1.

Further to the effects of coring, Piper [14] showed that annealing a $Pd_{60}Cu_{40}$ wt% membrane at 350 °C in 507 kPa of hydrogen pressure can almost double the diffusivity at room temperature when compared to annealing at the same temperature in a vacuum. Generally, annealing in the presence of hydrogen is beneficial for the Pd-Cu foil membrane in order to undo the compositional inhomogeneity caused by coring and facilitate the formation of the BCC equilibrium phase.

As temperature increased, it was revealed that the *n*-value of the Pd-Cu foil membrane deviated from Sieverts' law. Fig. 9 displays changes in the *n*-value with varying temperature for the Pd-Cu foil membrane. Between 350 and 375 °C, Sieverts' law is obeyed although, increasing the temperature yields a maximum *n*-value of 0.69 at 425 °C followed by a small decrease to 0.65 at 450 °C.

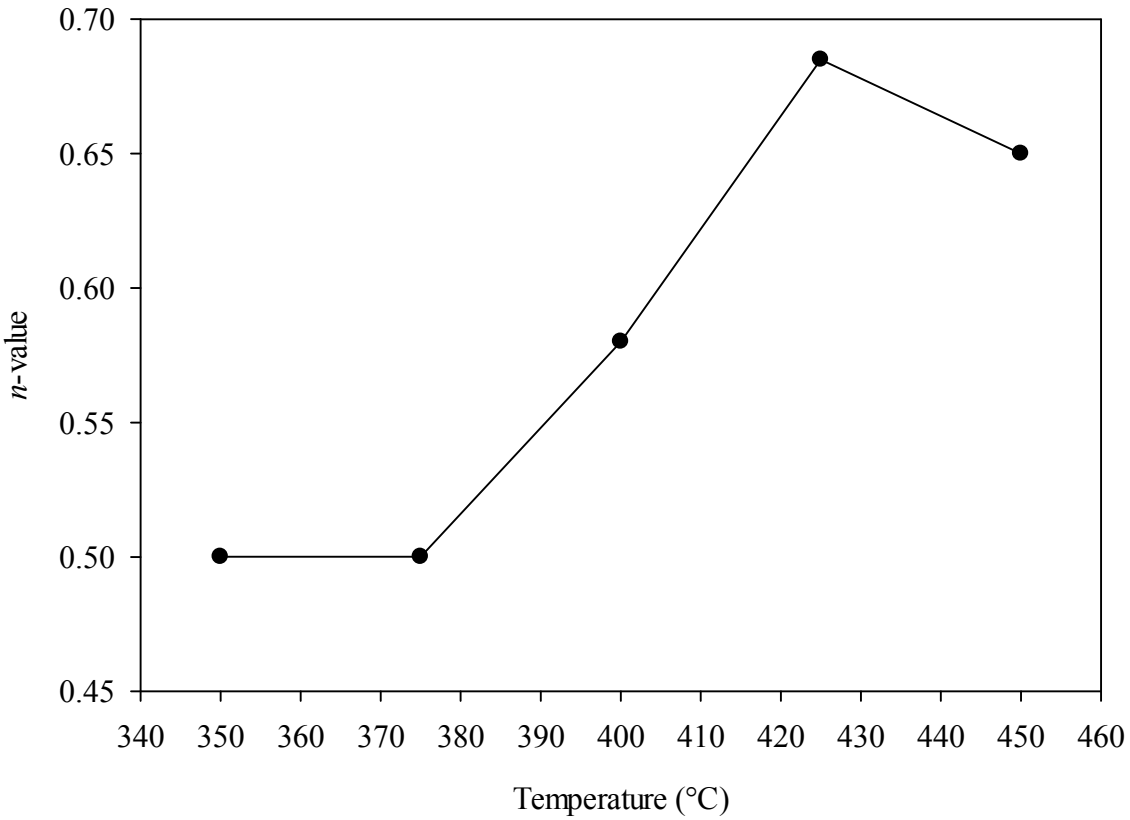

Fig. 9 Fluctuation in the *n*-value with temperature for the 31.0 µm thick Pd-Cu foil membrane.

Additional permeability measurements were performed on the Pd-Cu foil membrane by cycling from 250 to 700 °C following cycling from 50 to 450 °C to examine the effects of the disordered FCC phase on hydrogen permeability. Fig. 10 displays the results for the second cycle. The cycle pattern has the following sequence: A – B – C – D – E – A.

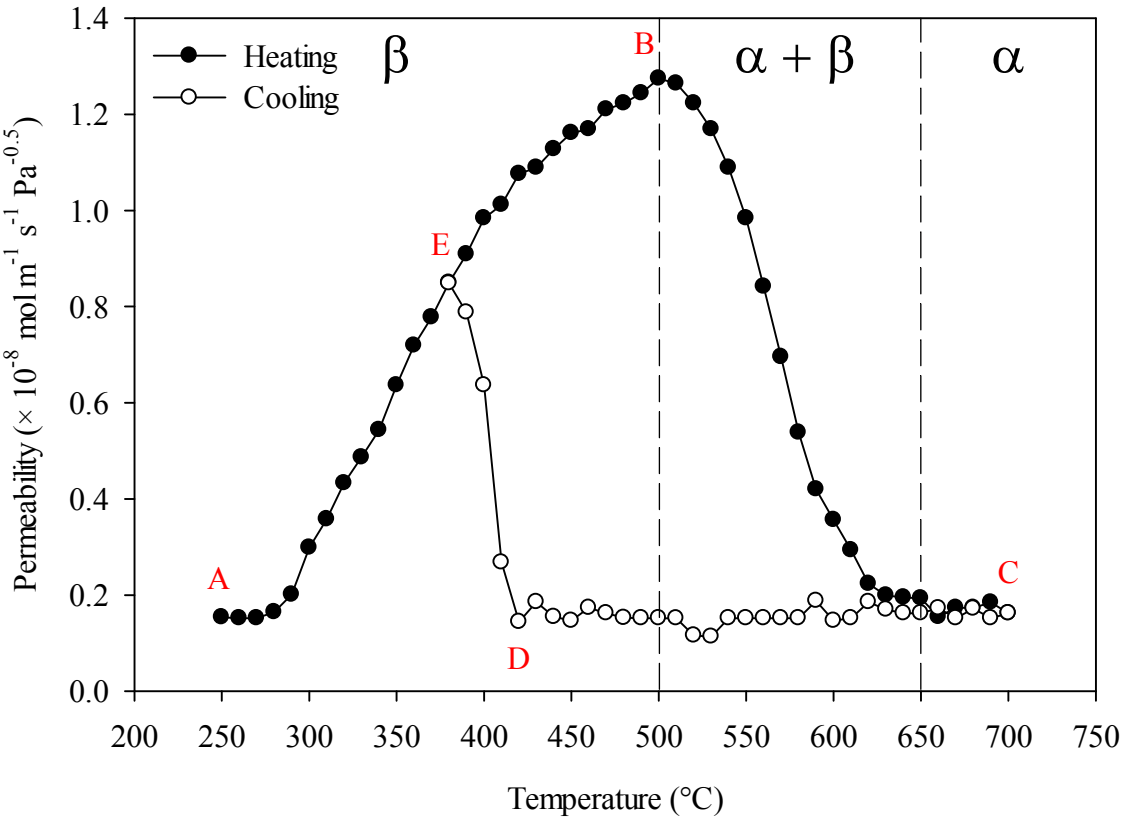

Fig. 10 Hydrogen permeability of the 31.0 µm thick Pd-Cu foil membrane against temperature in the second cycle between 250 and 700 °C. The applied hydrogen feed and permeate pressure was 445 kPa and 100 kPa, respectively. The phase boundaries are represented by the dashed lines indicating the FCC (α), BCC (β) and the α + β mixed phase regions that were derived from the phase transition temperatures displayed in Fig. 5.

The start of the cycle is denoted A and occurs at 250 °C and subsequently at B the hydrogen permeability reaches a maximum value that coincides with 500 °C. It is interesting to note that hydrogen permeation in the Pd-Cu foil membrane exceeded the detection limit of the MFC first at 250 °C during the second cycle up to 700 °C as opposed to 350 °C during the third cycle between 50 and 450 °C (Fig. 7). A hydrogen permeability of 6.36×10^{-9} mol m^{-1} s^{-1} $Pa^{-0.5}$ is achieved by the Pd-Cu foil membrane at 350 °C which lies within the literature range listed in Table 2. Furthermore, this hydrogen permeability value is more than a factor of four times higher relative to that displayed in Fig. 7. The overall increase in hydrogen permeability and decrease in the temperature at which hydrogen permeation is detected can be linked to the exposure of the membrane to higher temperatures for longer durations which can help remove the effects of coring created during alloy production.

The hydrogen permeability declines by almost a factor of eight times between B and C. As shown in Fig. 5, the low permeability FCC phase forms at 500 °C and at 650 °C the Pd-Cu foil membrane consists purely of this phase. The reduction in hydrogen permeability can be linked to the relatively low hydrogen diffusivity in the FCC phase ($< 2 \times 10^{-6}$ cm^2 s^{-1} at room temperature) in comparison to the BCC phase (4.6×10^{-5} cm^2 s^{-1} at room temperature) [14]. Kamakoti et al [37] have cited a similar observation whereby the transport of hydrogen between interstitial sites was modelled using density functional theory.

Piper [14] claims, without any data evidence, that hydrogen diffusivity is comparatively low in the FCC phase since the activation energy for this process is a factor of three times greater than in the BCC phase. This may be associated with the fact that the relatively small BCC unit cell contains a factor of three times more tetrahedral interstitial sites than the FCC phase [39] which would facilitate faster hydrogen transport between unit cells.

From C, D to E hydrogen permeation hysteresis is evident. This phenomenon has been associated with non-equivalent phase transformation that takes place in the mixed FCC + BCC region and it has also been hypothesised that the FCC(H) ⇋ BCC(H) phase transition is hindered by the presence of a metastable hydrogenated FCC Pd-Cu(H) phase [16]. The VTXRD results displayed in Fig. 4 and Fig. 6 give indication that the FCC phase is stable at temperatures lower than typically expected in either a helium or hydrogen atmosphere in the cooling stage of the cycle. This would imply that instead of a metastable hydrogenated FCC Pd-Cu(H) phase being responsible for the hydrogen permeation hysteresis shown in Fig. 10, it is suggested that rather in the present case the cooling rate has more of an effect since this influences the rate of phase transformation from the FCC phase to the BCC phase.

It is likely at E that the FCC phase has fully transformed to the high permeability BCC phase following which the curve proceeds to the conclusion of the cycle at A. It would appear that the effects of hydrogen permeation hysteresis could be alleviated by implementing a relatively slow and controlled cooling rate instead of the natural furnace cooling rate used during MPR testing.

Following the cycling up to 700 °C, *n*-value measurements were carried out on the Pd-Cu foil membrane for the purpose of verifying any changes caused by exposure to hydrogen at elevated temperatures. Fig. 11 reveals a reduction in the *n*-value from 0.58 to 0.52. Coring has had the effect of concentrating Pd atoms in the internal regions of the Pd-Cu foil membrane resulting in a Cu-rich surface. The existence of this Cu-rich surface will negatively impact the catalytic activity for hydrogen dissociation of the Pd-Cu foil membrane and would likely increase the *n*-value. Cycling of the Pd-Cu foil membrane to 700 °C in a hydrogen atmosphere will enable compositional homogenisation allowing Cu atoms to diffuse into the Cu-depleted internal region and consequently reduce the *n*-value to 0.5.

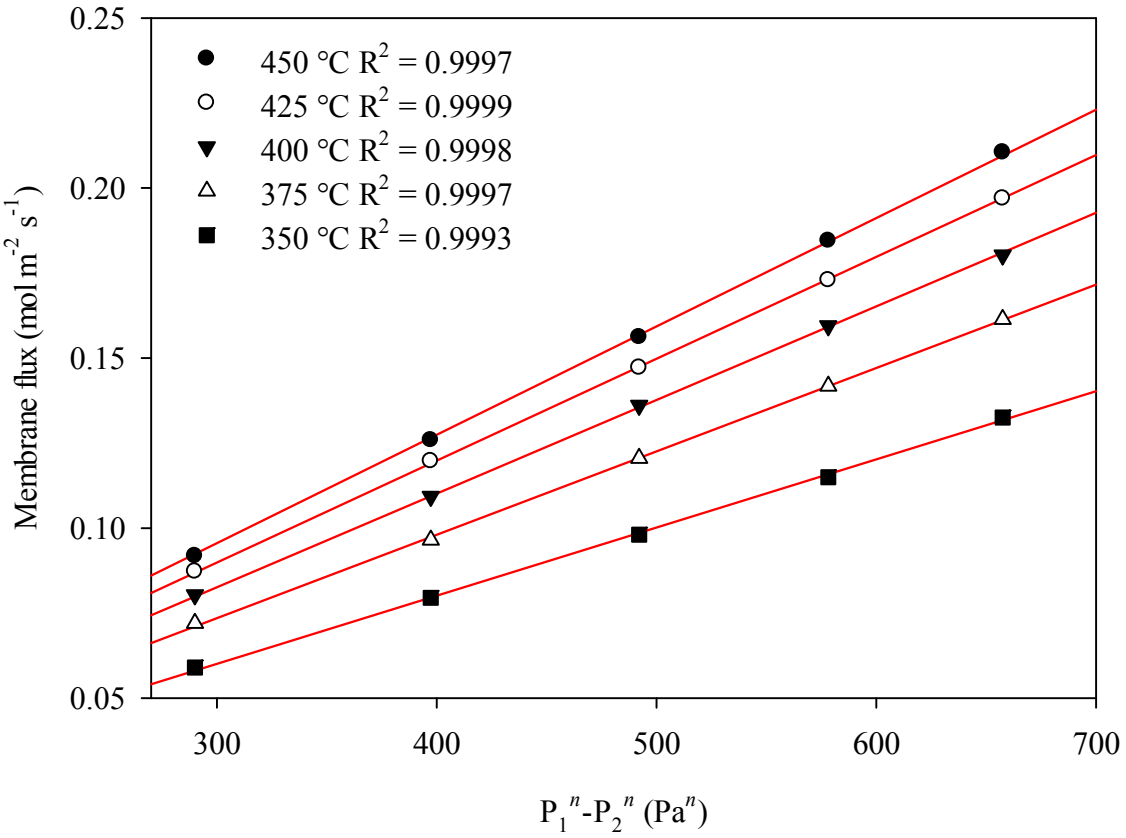

Fig. 11 Membrane flux against hydrogen differential pressure constrained to the best fit *n*-value of 0.52. The measurements were made on the Pd-Cu foil membrane subsequent to cycling between 250 and 700 °C in the MPR test.

The Pd-Cu foil membrane was then cycled from 250 to 450 °C subsequent to performing the two cycles between 250 and 700 °C demonstrating a noticeable increase in hydrogen permeability. In the third cycle from 250 to 450 °C, the Pd-Cu foil membrane attained a hydrogen permeability value at 350 °C of 6.98×10^{-9} mol m^{-1} s^{-1} $Pa^{-0.5}$ which is a 360% improvement upon the value achieved at the same temperature in the third cycle from 50 to 450 °C.

Eq. 6 and Eq. 7 show the new general permeability formulae (350 – 450 °C) derived for the Pd-Cu foil membrane using an *n*-value of 0.5 and best fit *n*-value of 0.52, respectively.

$$\Phi_{n=0.5} = (3.41 \times 10^{-7})\ mol\ m^{-1}\ s^{-1}\ Pa^{-0.5} \times exp\left(\frac{-19.86\ kJ\ mol^{-1}}{RT}\right) \quad \textbf{Eq. 6}$$

$$\Phi_{n=0.52} = (2.71 \times 10^{-7})\ mol\ m^{-1}\ s^{-1}\ Pa^{-0.52} \times exp\left(\frac{-19.86\ kJ\ mol^{-1}}{RT}\right) \quad \textbf{Eq. 7}$$

Cycling of the Pd-Cu foil membrane up to 700 °C under the conditions used during MPR testing has the effect of decreasing the E_Φ value from 51.09 kJ mol^{-1}, as displayed in Eq. 6 and Eq. 7, to 19.86 kJ mol^{-1} which is a 61% reduction. Moreover, the MPR test conditions used in this work have likewise decreased the Φ_0 value by an order of magnitude.

From the data presented by McKinley [8] for a $Pd_{60}Cu_{40}$ wt% foil membrane, an E_Φ value of 7.4 kJ mol^{-1} (300 – 400 °C) can be calculated; however, it should be noted that the accuracy of this activation energy is relatively low in this temperature range since it is based only on three reported hydrogen permeation data points recorded at 300, 350 and 400 °C. Furthermore, Matsumura [29] reports an E_Φ value of 6.1 kJ mol^{-1} (400 – 450 °C) for a $Pd_{60}Cu_{40}$ wt% foil membrane that dwelled between 400 and 450 °C for approximately 250 hours; it should be noted as well that this E_Φ value is based on only three reported hydrogen permeation data points recorded at 400, 425 and 450 °C. Fig. 12 shows that the *n*-value varies around 0.51 and at 450 °C increases slightly to 0.54.

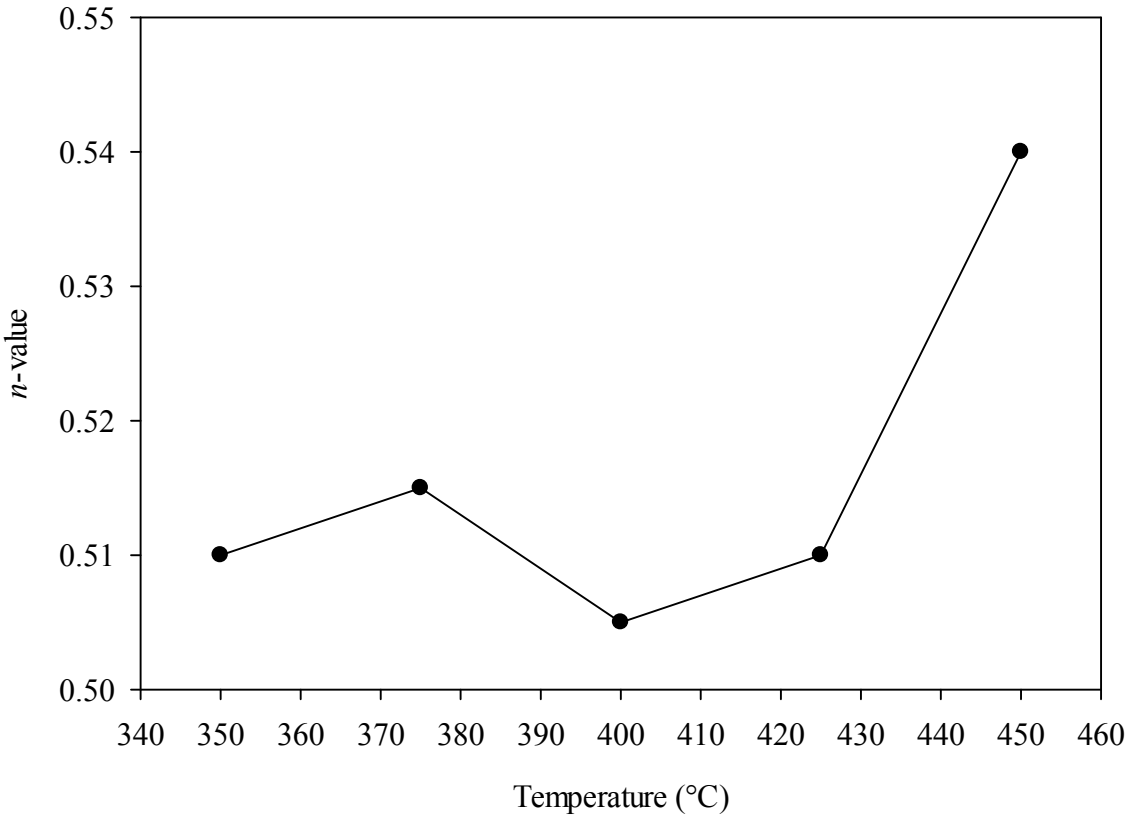

Fig. 12 Fluctuation in the *n*-value with temperature for the 31.0 µm thick Pd-Cu foil membrane after cycling from 250 to 700 °C during MPR testing.

3.3 Post-MPR characterisation

Following MPR testing, ex-situ XRD analysis was carried out on the Pd-Cu foil membrane in order to examine any phase changes brought on by the experimental conditions used. Fig. 13 shows an XRD pattern acquired for a Pd-Cu foil membrane that was cycled to a maximum temperature of 450 °C. Fig. 13(a) indicates that the feed side of Pd-Cu foil membrane contains just the BCC phase whereas Fig. 13(b) shows that the permeate side mostly contains the BCC phase with trace amounts of the FCC phase present as evidenced by the Pd-Cu(111)* diffraction peak.

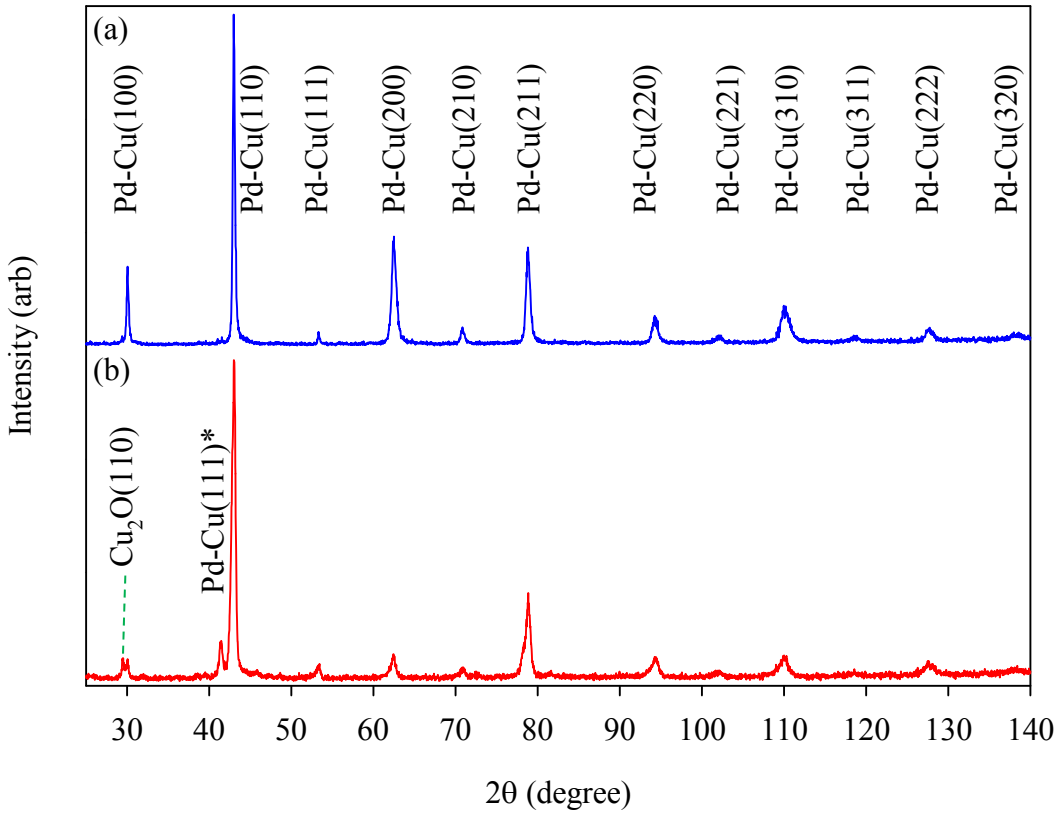

Fig. 13 XRD patterns acquired for the (a) feed side and (b) permeate side of the as-received Pd-Cu foil membrane following MPR testing. The Pd-Cu foil membrane was cycled to a maximum temperature of 450 °C. '*' denotes the diffraction peak associated with the FCC phase.

Fig. 14 displays the ex-situ XRD patterns acquired for the Pd-Cu foil membrane that had completed multiple cycles up to a maximum temperature of 700 °C with a hydrogen feed pressure of 445 kPa and permeate pressure of 100 kPa. The XRD pattern demonstrates that the Pd-Cu foil membrane contains a purely BCC phase on both sides. This is additional proof that exposure to elevated temperatures with a hydrogen feed pressure of 445 kPa and permeate pressure of 100 kPa anneals the Pd-Cu foil membrane and facilitates a total phase transformation from the FCC phase to the BCC equilibrium phase.

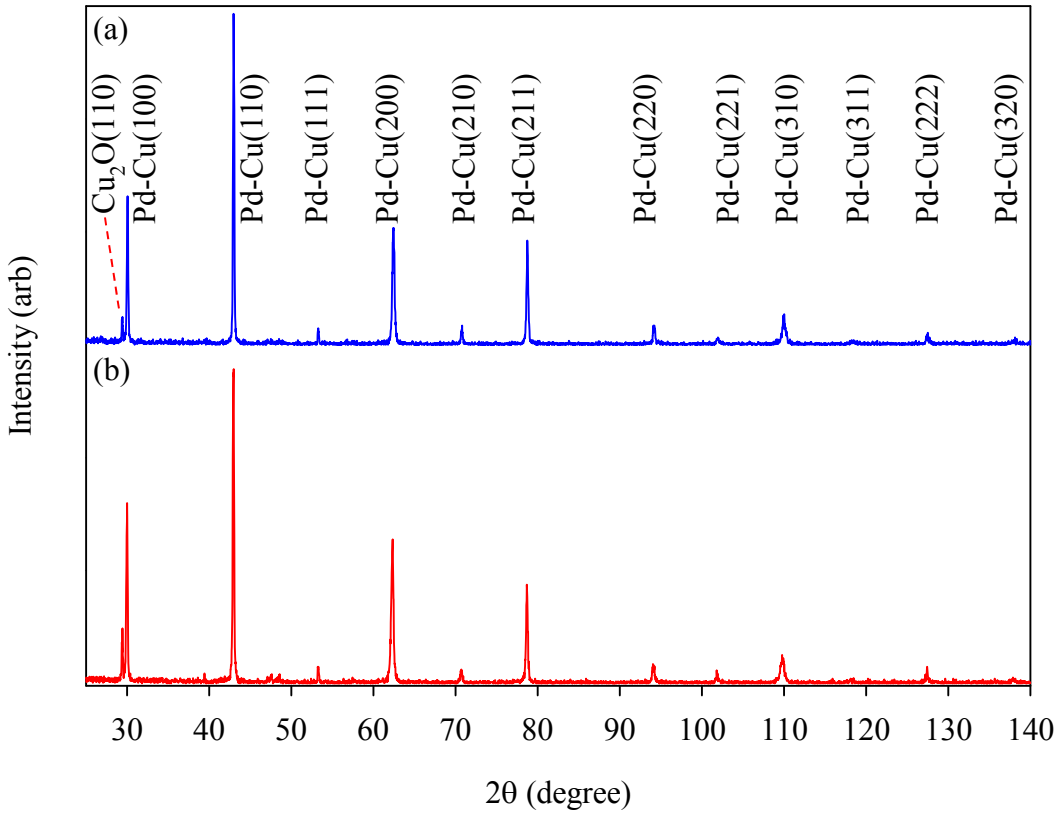

Fig. 14 XRD patterns acquired for the (a) feed side and (b) permeate side of the as-received Pd-Cu foil membrane following MPR testing. This Pd-Cu foil membrane had been cycled to a maximum temperature of 700 °C.

4 Conclusions

Hydrogen permeability was determined for an as-received Pd-Cu foil membrane that was cycled from 50 to 450 °C. During the third cycle, the hydrogen permeability at 450 °C for the Pd-Cu foil membrane was 5.59×10^{-9} mol m^{-1} s^{-1} $Pa^{-0.5}$, which is comparatively low when compared to literature data. Although, it was shown that the Pd-Cu foil membrane achieved relatively higher hydrogen permeability values with every consecutive cycle. Furthermore, it was discovered that cycling the Pd-Cu foil membrane to a maximum temperature of 700 °C resulted in the reduction of the E_Φ value by a factor of two and consequently decreased the n-value yielding an increased hydrogen permeability value of 1.19×10^{-8} mol m^{-1} s^{-1} $Pa^{-0.5}$ at 450 °C. This new hydrogen permeability value agrees well with the literature data [15, 37].

Coring was the probable culprit for the initially low hydrogen permeability values demonstrated by the Pd-Cu foil membrane. Coring probably happened in the as-received Pd-Cu foil due to quenching of the alloy in the molten state to room temperature which would have the effect of trapping the high temperature disordered FCC phase. Moreover, this produced inhomogeneity in the alloy composition since the relatively lower melting point constituent, Cu atoms in this instance, solidify first and move towards the external region of the alloy resulting in the majority of the Pd atoms concentrating towards the internal region.

Extended cycling and exposure to high temperatures in a hydrogen atmosphere was shown to be effective in homogenising the alloy composition of the Pd-Cu foil membrane and enhancing hydrogen permeation. A similar effect was reported by Krueger [38] for a Pd-Cu

foil membrane and it is suggested that annealing at temperatures near to the Cu melting point in a hydrogen containing atmosphere is capable of undoing the residual coring effects and thus substantially increasing hydrogen permeability.

The Pd-Cu foil membrane cycled up to 700 °C exhibited permeation hysteresis. Yuan [16], associates this phenomenon to the existence of a metastable hydrogenated FCC Pd-Cu(H) phase which retards the FCC(H) ⇋ BCC(H) phase transition. Interestingly, VTXRD analysis conducted on the Pd-Cu foil samples reveal that the FCC phase is stable at temperatures lower than typically expected in either a helium or hydrogen atmosphere. Hence, in the present case it is suggested that the presence of the FCC phase at lower than normal temperatures is most likely linked to the cooling rate instead of the occurrence of a metastable hydrogenated FCC Pd-Cu(H) phase. Reduced cooling rates will enable sufficient time for the FCC phase to transform to the BCC phase under equilibrium conditions.

Moreover, VTXRD analysis performed on the Pd-Cu foil samples revealed that a hydrogen pressure of 445 kPa shifts the BCC | FCC + BCC and FCC + BCC | FCC phase boundaries towards relatively higher temperatures and the Pd-rich end of the Pd-Cu phase diagram. This observation agrees well with the findings described by Piper [14] and explains the ability of the BCC phase to occur outside of the limits of the phase boundaries displayed in Pd-Cu phase diagram by Subramanian and Laughlin [13].

Acknowledgements

The authors are thankful to Johnson Matthey Noble Metals (Royston, UK) for the supply of cold rolled Pd-Cu foils. The support from the EPSRC (United Kingdom) Doctoral Training Centre (DTC) in Hydrogen, Fuel Cells and their Applications (EP/G037116/1) is also gratefully acknowledged, as is the support from the research group of Professor David Book, School of Metallurgy and Materials, University of Birmingham.

References

[1] L. Barelli, G. Bidini, F. Gallorini, S. Servili, Hydrogen production through sorption-enhanced steam methane reforming and membrane technology: A review, Energy, 33 (2008) 554-570.
[2] J.D. Holladay, J. Hu, D.L. King, Y. Wang, An overview of hydrogen production technologies, Catalysis Today, 139 (2009) 244-260.
[3] A. Faur Ghenciu, Review of fuel processing catalysts for hydrogen production in PEM fuel cell systems, Current Opinion in Solid State and Materials Science, 6 (2002) 389-399.
[4] A.G. Knapton, Palladium alloys for hydrogen diffusion membranes, Platinum Metals Review, 21 (1977) 44-50.
[5] S. Adhikari, S. Fernando, Hydrogen membrane separation techniques, Industry & Engineering Chemistry Research, 45 (2006) 875-881.
[6] S.N. Paglieri, J.D. Way, Innovations in palladium membrane research, Separation and Purification Methods, 31 (2002) 1-169.
[7] D.L. McKinley, Metal alloy for hydrogen separation and purification, U.S. Patent 3,350,845 (1967).

[8] D.L. McKinley, Method for hydrogen separation and purification, U.S. Patent 3,439,474 (1969).
[9] K.S. Rotherberg, B.H. Howard, R.P. Killmeyer, M.V. Ciocco, B.D. Morreale, R.M. Enick, Palladium-copper alloy membrane performance under continuous exposure, in: National Hydrogen Association, Washington, DC, 2005, pp. 1-10.
[10] N. Pomerantz, Y.H. Ma, Effect of H_2S on the performance and long-term stability of Pd/Cu membranes, Industrial & Engineering Chemistry Research, 48 (2009) 4030-4039.
[11] N. Pomerantz, Y.H. Ma, Novel method for producing high H_2 permeability Pd membranes with a thin layer of the sulfur tolerant Pd/Cu fcc phase, Journal of Membrane Science, 370 (2011) 97-108.
[12] B. Morreale, M. Ciocco, B. Howard, R. Killmeyer, A. Cugini, R. Enick, Effect of hydrogen-sulfide on the hydrogen permeance of palladium–copper alloys at elevated temperatures, Journal of Membrane Science, 241 (2004) 219-224.
[13] P. Subramanian, D. Laughlin, Cu-Pd (copper-palladium), Journal of Phase Equilibria, 12 (1991) 231-243.
[14] J. Piper, Diffusion of hydrogen in copper-palladium alloys, Journal of Applied Physics, 37 (1966) 715-721.
[15] B. Howard, R. Killmeyer, K. Rothenberger, A. Cugini, B. Morreale, R. Enick, F. Bustamante, Hydrogen permeance of palladium–copper alloy membranes over a wide range of temperatures and pressures, Journal of Membrane Science, 241 (2004) 207-218.
[16] L. Yuan, A. Goldbach, H. Xu, Permeation hysteresis in PdCu membranes, Journal of Physical Chemistry B, 112 (2008) 12692-12695.
[17] M. Li, Z. Du, C. Guo, C. Li, A thermodynamic modeling of the Cu–Pd system, Calphad, 32 (2008) 439-446.
[18] J. Völkl, G. Alefeld, Diffusion of hydrogen in metals, in: G. Alefeld, J. Völkl (Eds.) Hydrogen in metals I, Springer, Berlin, 1978, pp. 321-348.
[19] P. Kamakoti, D.S. Sholl, A comparison of hydrogen diffusivities in Pd and CuPd alloys using density functional theory, Journal of Membrane Science, 225 (2003) 145-154.
[20] W. Huang, S.M. Opalka, D. Wang, T.B. Flanagan, Thermodynamic modelling of the Cu–Pd–H system, Calphad, 31 (2007) 315-329.
[21] N. Fukumuro, M. Yokota, S. Yae, H. Matsuda, Y. Fukai, Hydrogen-induced enhancement of atomic diffusion in electrodeposited Pd films, Journal of Alloys and Compounds, 580, Supplement 1 (2013) S55-S57.
[22] T.B. Flanagan, C.-N. Park, Hydrogen-induced rearrangements in Pd-rich alloys, Journal of Alloys and Compounds, 293 (1999) 161-168.
[23] C. Decaux, R. Ngameni, D. Solas, S. Grigoriev, P. Millet, Time and frequency domain analysis of hydrogen permeation across PdCu metallic membranes for hydrogen purification, International Journal of Hydrogen Energy, 35 (2010) 4883-4892.
[24] A. Goldbach, L. Yuan, H. Xu, Impact of the fcc/bcc phase transition on the homogeneity and behavior of PdCu membranes, Separation and Purification Technology, 73 (2010) 65-70.
[25] B.D. Cullity, Elements of X-ray diffraction, Addison-Wesley Publishing Company, Reading, Massachusetts, 1956.
[26] L. Vegard, Die konstitution der mischkristalle und die raumfüllung der atome, Zeitschrift für Physik A Hadrons and Nuclei, 5 (1921) 17-26.
[27] N. Al-Mufachi, S. Nayebossadri, J. Speight, W. Bujalski, R. Steinberger-Wilckens, D. Book, Effects of thin film Pd deposition on the hydrogen permeability of Pd 60 Cu 40 wt% alloy membranes, Journal of Membrane Science, 493 (2015) 580-588.
[28] F.W. Jones, C. Sykes, The transformations in the copper-palladium alloys, Journal of the Institute of Metals, 65 (1939) 419-433.

[29] Y. Matsumura, A basic study of high-temperature hydrogen permeation through bcc Pd–Cu alloy foil, Separation and Purification Technology, 138 (2014) 130-137.
[30] L. Yuan, A. Goldbach, H. Xu, Segregation and H_2 transport rate control in body-centered cubic PdCu membranes, Journal of Physical Chemistry B, 111 (2007) 10952-10958.
[31] S. Nakahara, J.A. Abys, S.M. Abys, Room-temperature diffusion-induced grain boundary migration in the fine-grained Pd side of Cu-Pd diffusion couples, Materials Letters, 2 (1983) 155-159.
[32] A. Zetkin, G. Kagan, A. Varaksin, E. Levin, J. Caffrey, Diffusion and penetrability of deuterium in the alloy Pd−53 at.% Cu, Soviet Physics Solid State, 34 (1992) 83-85.
[33] M. Hansen, K.P. Anderko, R.P. Elliott, Constitution of binary alloys, McGraw-Hill, New York, 1958.
[34] E. Hayashi, Y. Kurokawa, Y. Fukai, Hydrogen-induced enhancement of interdiffusion in Cu-Ni diffusion couples, Physical Review Letters, 80 (1998) 5588-5590.
[35] Y. Fukai, Formation of superabundant vacancies in M–H alloys and some of its consequences: a review, Journal of Alloys and Compounds, 356 (2003) 263-269.
[36] T.L. Ward, T. Dao, Model of hydrogen permeation behavior in palladium membranes, Journal of Membrane Science, 153 (1999) 211-231.
[37] P. Kamakoti, B.D. Morreale, M.V. Ciocco, B.H. Howard, R.P. Killmeyer, A.V. Cugini, D.S. Sholl, Prediction of hydrogen flux through sulfur-tolerant binary alloy membranes, Science, 307 (2005) 569-573.
[38] C. Krueger, Method of improving and optimizing the hydrogen permeability of a palladium-copper membrane and novel membranes manufactured thereby, U.S. Patent 6,372,363 B1 (2002).
[39] M.D. Dolan, Non-Pd BCC alloy membranes for industrial hydrogen separation, Journal of Membrane Science, 362 (2010) 12-28.